REPORT DOCUMENTATION PAGE

1. REPORT DATE *(DD-MM-YYYY)*	2. REPORT TYPE	3. DATES COVERED *(From - To)*
13-11-2014	Final	11-April-2013 to 10-April-2014

4. TITLE AND SUBTITLE	
Enhanced Reciprocal Interactions between Molecular Stresses and Optoelectronic Energy Transfers for High Efficiency Long Life Devices Based on Conjugated Polymers	**5a. CONTRACT NUMBER** FA2386-13-1-4026
	5b. GRANT NUMBER Grant AOARD-134026
	5c. PROGRAM ELEMENT NUMBER 61102F

6. AUTHOR(S)	
Prof. Arnold Chang-Mou Yang	**5d. PROJECT NUMBER**
	5e. TASK NUMBER
	5f. WORK UNIT NUMBER

7. PERFORMING ORGANIZATION NAME(S) AND ADDRESS(ES)	8. PERFORMING ORGANIZATION REPORT NUMBER
National Tsing Hua University 101, Kuang Fu Rd, Sec 2 Hsinchu 30043 Taiwan	N/A

9. SPONSORING/MONITORING AGENCY NAME(S) AND ADDRESS(ES)	10. SPONSOR/MONITOR'S ACRONYM(S)
AOARD UNIT 45002 APO AP 96338-5002	AFRL/AFOSR/IOA(AOARD)
	11. SPONSOR/MONITOR'S REPORT NUMBER(S) AOARD-134026

12. DISTRIBUTION/AVAILABILITY STATEMENT

Distribution A: Approved for public release. Distribution is unlimited

13. SUPPLEMENTARY NOTES

14. ABSTRACT
This report describes an investigation into the effects of mechanical deformation on photoluminescence (PL) behavior for the neat conjugated polymers: poly[2-methoxy-5-(2-ethylhexyloxy)-1,4-phenylenevinylene] (MEH-PPV) and polythiophenes (P3HT, P3BT, P3EHT). This study used a unique bilayer stretching method where the thin conjugated polymer was drawn into local deformation zones at very high local mechanical strain (~300%) on top of glassy polystyrene film. It was found that very large PL enhancement (i.e., as high as ~60x) was observed for neat MEH-PPV polymers during mechanical deformation, which was comparable to that observed in the dilute systems. In contrast, for crystalline neat P3HT films, bilayer stretching resulted in insignificant PL enhancement. Substantial PL enhancement emerged (~15x), however, when strong intermolecular interactions were obstructed by bulky side-groups (in P3EHT). The results indicated that once conjugated polymer chains are effectively stretched and thus confined by mechanical stresses, suppression of electron-phonon coupling can prevail in the neat resins to give rise to the dramatic efficiency enhancements. Such enhancement was not found to be exploited via imprinting methods unless proper precautions were taken during mechanical strain. The reciprocal relation that mechanical behavior of conjugated polymer chains can be controlled by light absorption was also explored. By shining light through an optical mask, the movements of conjugated polymers in a thin film can be manipulated to form patterns in accordance to that on the mask. Electro-poling also produced molecular stress effects on efficiency enhancement in conjugated polymers.

15. SUBJECT TERMS

Conjugated Polymers, Nanophotonics, Photoluminenscence, Mechanical Strain, Thin Films

16. SECURITY CLASSIFICATION OF:			17. LIMITATION OF ABSTRACT	18. NUMBER OF PAGES	19a. NAME OF RESPONSIBLE PERSON
a. REPORT	b. ABSTRACT	c. THIS PAGE			Kenneth Caster, Ph.D.
U	U	U	SAR	32	**19b. TELEPHONE NUMBER** *(Include area code)* +81-42-511-2000

Standard Form 298 (Rev. 8/98)
Prescribed by ANSI Std. Z39.18

Final Report for AOARD 134026

Enhanced Reciprocal Interactions between Molecular Stresses and Optoelectronic Energy Transfers for High Efficiency Long Life Devices Based on Conjugated Polymers

Oct. 15, 2014

Name of Principal Investigators: Arnold Chang-Mou Yang
 – e-mail address : acyang@mse.nthu.edu.tw
 – Institution : Department of Materials Science and Engineering, National Tsing Hua University, Hsinchu, Taiwan
 – Mailing Address : 101, Kuang Fu Road, Hsinchu City, Taiwan
 – Phone : +886 (3) 572 0792
 – Fax : +886 (3) 572 2366

Period of Performance: 06/15/2013 – 04/14/2014

Abstract:
        Evidence of massive enhancements of the quantum efficiencies of conjugated polymers by molecular stresses had so far been limited to diluted systems, casting doubts on the universal validity of the mechanical stress effect and impairing the likelihood of practical applications. The effects on the PL behavior by mechanical deformation of the neat conjugated polymers of MEH-PPV and polythiophenes (P3HT, P3BT, P3EHT) were therefore studied herein by using a unique bilayer stretching method where the thin conjugated polymer was stretched on top of a glassy polymer films (polystyrene, PS) that was undergoing local deformation, drawing the conjugated polymer chains into the local deformation zones of very large local mechanical strains (~300% strain). It was found that for neat MEH-PPV polymers, very large PL enhancements were observed during the mechanical deformations which were comparable to those observed in the diluted systems, with a magnitude as high as ~60 fold. For crystalline neat P3HT films, in contrast, the PL enhancements resulted from the bilayer stretching were insignificant. Substantial PL enhancements emerged (~15 folds), however, when the strong intermolecular interactions were obstructed by bulky side-groups (in P3EHT). The results indicate that once the conjugated polymer chains are effectively stretched and thus confined by mechanical stresses, suppression of electron-phonon coupling can prevail in the neat resins to give rise to the dramatic efficiency enhancements. The intermolecular interactions, such as molecular aggregates and crystallites, however, can hamper the operation of this mechanical effect. The massive enhancements of optoelectronic efficiencies were found related to energy transfer characteristics in the femto-second regime in that the emission energy red-shifted substantially slower when the polymer chains were stretched, which is consistent with the operation of suppression of electron-phonon coupling for the efficiency enhancements.
        The efficiency enhancement via mechanical stress was found not to be exploited via imprinting methods unless proper precautions were made. The ineffectiveness of using the imprinting method was attributed to the relaxation of the mechanical stress during and after the imprinting.
        As a corollary of the mechano-optical effect, the reciprocal relation that mechanical behavior of conjugated polymer chains can be controlled by light absorption was explored. By shining light through an optical mask, the movements of conjugated polymers in a thin

film can be manipulated to form nice patterns in accordance to that on the mask. The macromolecular flows can be altered and even reversed by changing the concentration of the conjugated polymers in the films. The behavior was explained satisfactorily by the increased molecular stiffness induced by light absorption of the conjugated polymer. These results may serve as a good illustration of macromolecular movement control by selected area lighting.

Electro-poling, which are compatible with the current manufacturing processes of optoelectronic and semiconducting devices, was found able to produce the molecular stress effect of efficiency enhancements in conjugated polymers. Poling increased the efficiency although it competed with an electrets effect that could separate excitons and thus led to lower PL efficiencies. The latter, however, posed no problems for solar cells aplications. Furthermore, the molecular dipoles composed of π-electrons delocalized along the backbones of original conjugation lengths were found to dominate the molecular rearrangements induced by poling.

Finally, since conjugated polymers are rigid-rod macromolecules and hence would behave differently, from that of the more flexible polymers such as PS, when packed into ultrathin solid films for optoelectronic devices. The molecular packing of conjugated polymers in ultrathin films was hence explored by measuring the residual stresses and the through-thickness density distribution. Preliminary results have shown that the methodology taken is promising.

Introduction:

Conjugated polymers are promising candidates for next-generation optoelectronics and semiconductors owing to their low cost and unique properties. However, low quantum efficiency is still limiting the prospects of their applications. Despite many years of study, the underlying physics behind this deficiency is still elusive. One important physical factor, which is often ignored, is the influence of electron-phonon interactions operative in the mechanically soft linear polymer chains. The electron-phonon interactions, referring to the mechanical deformations coupling with local electronic excitations, in fact, form the fundamental framework of the Franck-Condon Principle (Fig. 1) that has long been used to explain energy dissipation during photoexcitation and de-excitation processes where the sub-states of each energy state of the organic molecules are attributed to the series of molecular vibrations coupling with the electronic eigenfunctions. Another iconic example is the non-radiative decay pathways that cause efficiency reduction in the general emission processes.
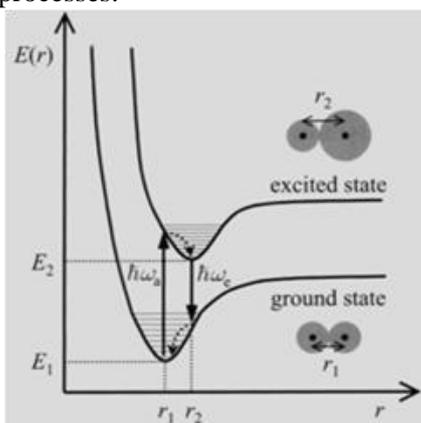
Figure 1. A schematic depiction of how mechanical interactions dissipate the absorbed energy during the photoexcitation and de-excitation processes in the so-called Franck-Condon cycle.

Despite its importance, the coupling between the molecular mechanical properties and the optoelectronic behavior has seldom been addressed when practical issues of quantum efficiencies were discussed and explored. We recently demonstrated that the quantum efficiency of conjugated polymers can be dramatically enhanced by mechanical stresses exerting on the molecular backbones: (1) stretching via local deformation (crazing or shear yielding) the molecules diluted in optically inert network (*ACS Nano* **2011**), (2) stretch the molecules

2

confined in ultrathin films by capillary forces in dewetting. (*ACS Nano* **2013**), (3) single-molecule MEH-PPV systems (*ACS Photonics*, in revision.), and (4) light-induced changes of molecular mechanical behavior in dewettting- a reciprocal effect (*Macromolecules* **2013**).

These works, however, were focusing on the aspect of mechano-optical interactions by using samples of dilute conjugated polymers in an optically inert matrix where the intermolecular effects of aggregation and crystallization played only minor roles. In these dilute systems, mechanical stress has been successfully demonstrated to dramatically enhance optoelectronic efficiency of conjugated polymers. The mechanical stress effect dwindles in the conjugated polymer systems where the molecules are concentrated and have opportunity to overlap with one another. However, sufficiently high concentration of conjugated polymer is required for the purpose of optoelectronic device applications. Can and how the conjugated molecules in concentrated systems undergo stress-enhanced quantum efficiencies? Another practical question to be faced is how to introduce mechanical stresses in the molecular segments in concentrated systems of conjugated polymers for device manufacturing? Can we use nanoimprinting, different pulling method such as bilayer local necking, or electric poling?

Furthermore, application of mechanical stresses can lead to reduction of exciton quenching for conjugated polymers (as illustrated in the case of dewetting, by the long-range van der Waals interactions), indicating that electron-phonon coupling play a fundamental role in exciton formation and exciton behavior. This, however, is to be confirmed by a direct mechanical stretching experiment. Moreover, further ultrafast experiments in the sub-pico-second range are required in order to probe the energy transfer process following molecular excitation.

Finally, as the reciprocal effect of the stress-induced PL, light (exposure, absorption) may be used to control polymer segmental motions. It is important to ask can we introduce molecular deformation (segmental scales) for any efficiency enhancement? And, can we use light to pattern dewetting for purpose of device making? Separately, since conjugated polymers are rigid-rod macromolecules, they have distinct solution and intermolecular behavior. Hence, it is necessary to explore how the conjugated polymer molecules are packed into the ultrathin films, how these molecular aggregates form, and how energy is transferred in systems where the molecular aggregates prevail? These items constitute the research focuses of this research endeavor reported here.

Experiments, Results and Discussions:

1. Efficiency Enhancements in Stretched Neat (or Concentrated) Conjugated Polymers

A. <u>Stretching Neat MEH-PPV and Polythiophenes</u>
Before exploring the mechanical effect on the optoelectronic properties of conjugated polymers in the highly concentrated and pristine regime, the mechanical behavior was first examined.

It was found that the pristine films of MEH-PPV were very fragile, undergoing catastrophic fracture at low mechanical strain around 0.5% via craze breakdown.

For the neat P3HT, uniform ductile deform showing no sign of local deformation or fracture (Fig. 2). The PL intensity, however, did not consistently increase with deformation (Fig. 3). The complicated behavior clearly was heavily influenced by molecular aggregation as well as crystallization.

3
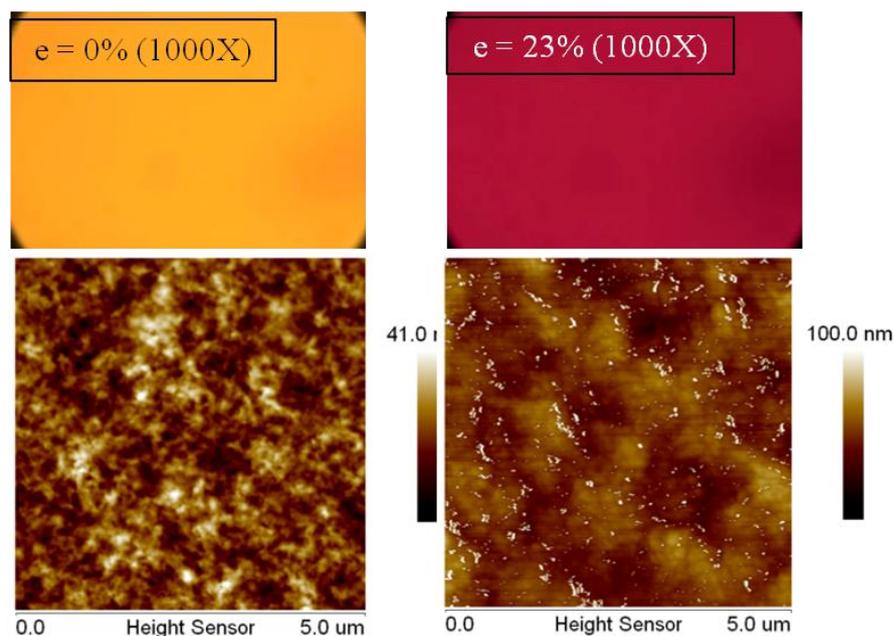
Figure 2. OM and AFM topographic micrographs of the neat P3HT (55kg/mol.) films (~0.25 μm) before (strain = 0) and after tensile stretching (strain = 23%).
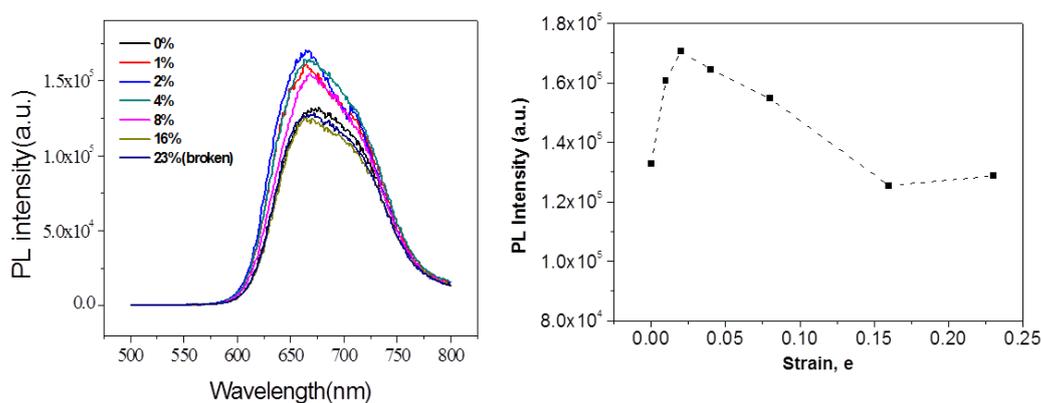
Figure 3. The PL spectra and the peak PL intensity of the stretched P3HT as a function of applied strain.

B. Stretching the Neat MEH-PPV in a Bilayer Local Deformation:

In order to solve the hurdle of mechanical fragility of the MEH-PPV, a bilayer stretching experiment was implemented in that a thin layer of the conjugated polymer (thickness $\tau = 10$, 20, or 30 nm) was deposited on the surface of a polystyrene (PS, M=2 Mg/mol., $\tau \sim 0.4\mu$m) (Fig. 4) after the PS film was bonded onto a piece of ductile copper grid (Fig. 5) designed for non-relaxation stretching. The bonding between the MEH-PPV film and the PS was controlled by solvent annealing, monitored by thickness change during the sorption process, and ensured by subsequent mechanical analysis.

4
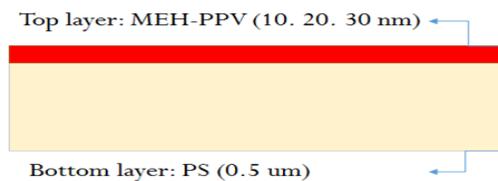
Figure 4. A schematic cross-section view of the bilayer sample.
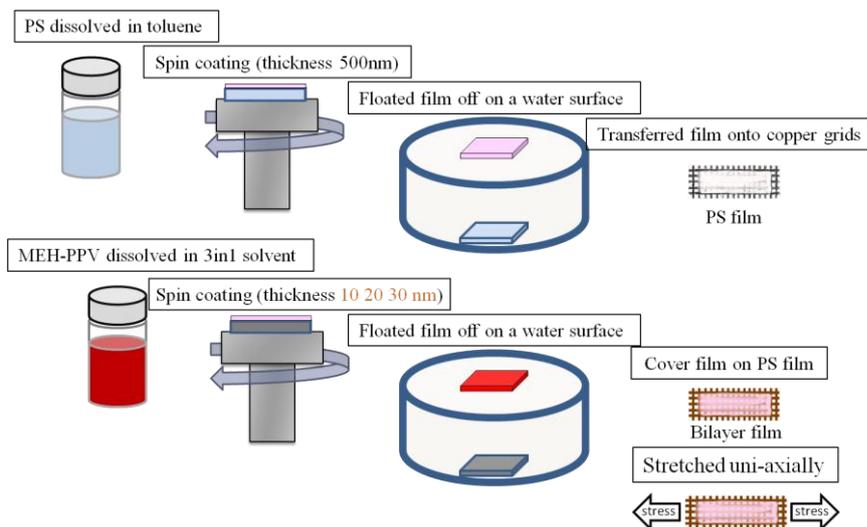
Figure 5. Schematic depiction of the preparation of the bilayer sample.

Figure 6. The OM micrographs of the stretched bilayer samples containing the neat MEH-PPV film for various strains.
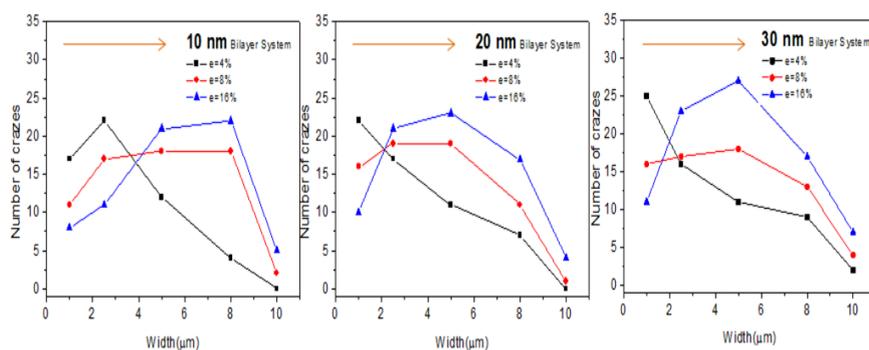
Figure 7. Population distribution of the crazes versus craze width for various applied strain.

Upon stretching, the PS film with the thin MEH-PPV coating layer developed the local deformation zones of crazes (Fig. 6). The craze number and width increased with the external strain increased. The population distribution of the crazes was determined, as shown in Fig. 7, for various applied strains. The craze topography was further examined under an AFM (Fig. 8) to reveal its characteristic microstructure and examine the necking behavior. The topography in the depressed bilayer regions exhibited the fibrillar structure (Fig. 9) similar to that in single-layer PS crazes, indicating that the meniscus instability of the PS molecules triggered by the tensile stress had effectively pulled along the MEH-PPV into local deformation. Consistently, from the local depths varying with the zone width of the depressed regions, micro-necking was clearly operative during the local deformation in the bilayer film (Fig. 10).
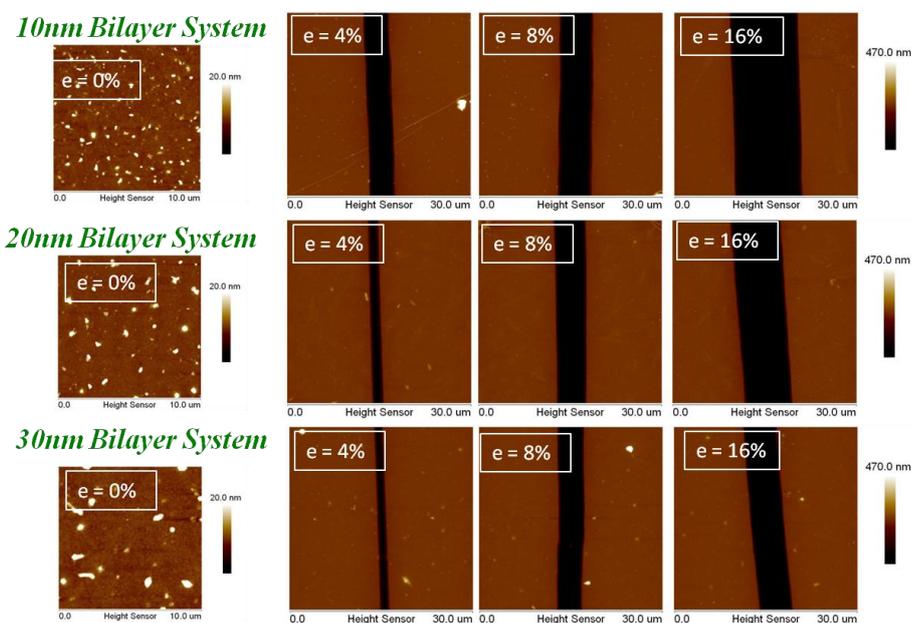
Figure 8. The AFM topographic micrographs of the bilayer samples before and after the stretching.

Pure PS single layer System

Fibrillated structure

Oriented
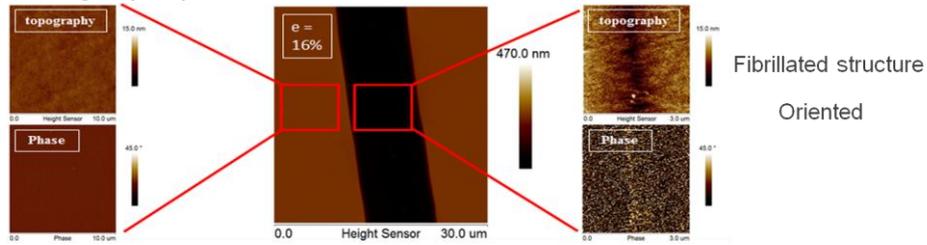
10 nm MEH-PPV Bilayer System

Fibril-like structure

Oriented
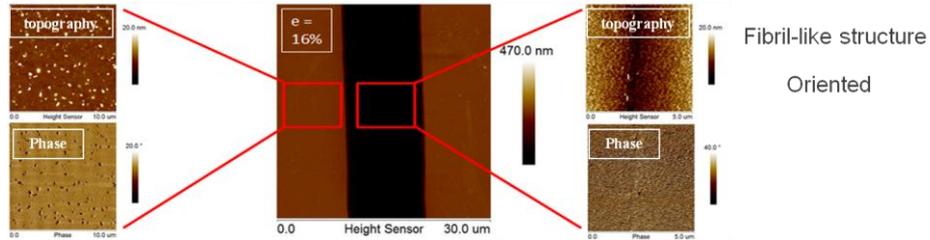
Figure 9. Enlarged AFM micrographs of the crazes in the bilayer samples showing the fibrillar microstructure of the micro-necked regions (the crazes).

τ =10 nm τ =20 nm τ = 30 nm

Single Layer - 0.5 um pure PS film
Bilayer -10nm 100% MEH-PPV/ 0.5um 100% PS
Bilayer -20nm 100% MEH-PPV/ 0.5um 100% PS
Bilayer -30nm 100% MEH-PPV/ 0.5um 100% PS

h: film thickness

τ: critical depth, known from AFM

$h_{MEH-PPV}$

τ_{PS}

$\tau_{MEH-PPV}$

d
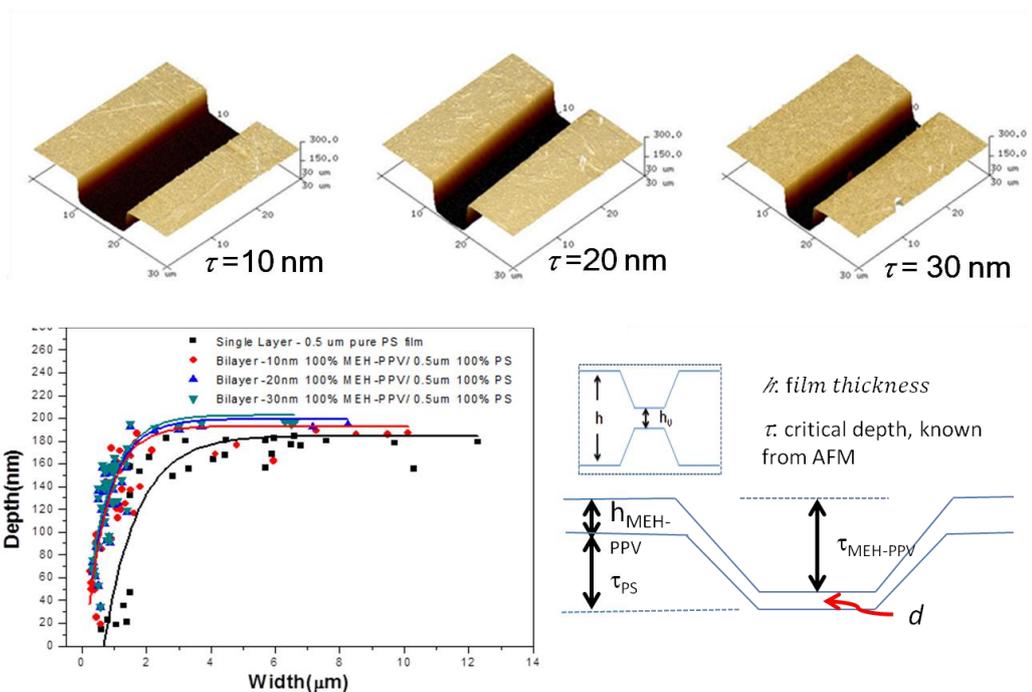
Figure 10. The behavior of the craze depth increasing with craze width until it saturates above the critical width reveals a micro-necking behavior.

The local stress and strain in the local deformation zones can be calculated from the AFM topography using the Bridgman's necking theory and G'sell and Marquez-Lucero model for plastic deformations. For micro-necking in the bilayer, local stress, strain, and strain rate distributions inside the crazes can be obtained. The tensile stress (σ_t) and the true tensile strain (ε) were respectively

7

$$\sigma_t = \frac{\beta}{\tau_0 w} F = \frac{E e_c \tau}{\tau} \beta \quad , \quad \varepsilon = \ln\left(\frac{\tau_0}{\tau}\right) - \frac{1}{3} \ln v_f + e_c$$

and the correcting factor β is

$$\beta = \left[\sqrt{1 + \frac{4R}{\tau}} \ln\left(1 + \frac{\tau}{2R} + \sqrt{\frac{\tau}{R}\left(1 + \frac{\tau}{4R}\right)}\right) - 1 \right]^{-1}$$

where F is the tension force, φ is the local neck thickness, R is the radius of the necking curvature, w is the neck length (i.e., the width of the deformation zone), τ_0 is the film thickness, τ is the half film thickness, E is the Young's modulus, e_c is the critical strain for the necking, and v_f is the volume fraction of the necked region. The distributions of the stress and strain rate inside the crazes are shown in Fig. 11. The stress outside the crazes was elastic and equal to the critical strain e_c multiplied with the Young modulus of the MEH-PPV.

Also shown in Fig. 11 is the inter-relation between the local stress versus local strain for the mechanical drawing for various samples. Generally, the local tensile stress increased with the craze width (Fig. 12).

By assuming that the drawing of the relatively thick PS layer ($\tau = 0.4\mu m$) was not affected by the thin MEH-PPV ($\tau = 10 - 30$ nm), and that the local stress in the bilayer was the sum of that of each layer that was linearly proportional to the average strain determined from necking thinning by AFM, the average stress operative in each of the MEH-PPV layer was calculated to be 215 MPa, 156 MPa, and 110 MPa, respectively for the 10 nm, 20 nm, and 30 nm MEH-PPV layer. The stress exerting on the PS layer was 125 MPa. These calculations were average values while the stress in fact should also varied along the thickness direction crossing the PS and MEH-PPV layers. For the sake of simplicity, this thickness dependence of stress was neglected here. Consistently, the average local pulling stress for the local deformation in the MEH-PPV layer increased with as its layer thickness decreased.
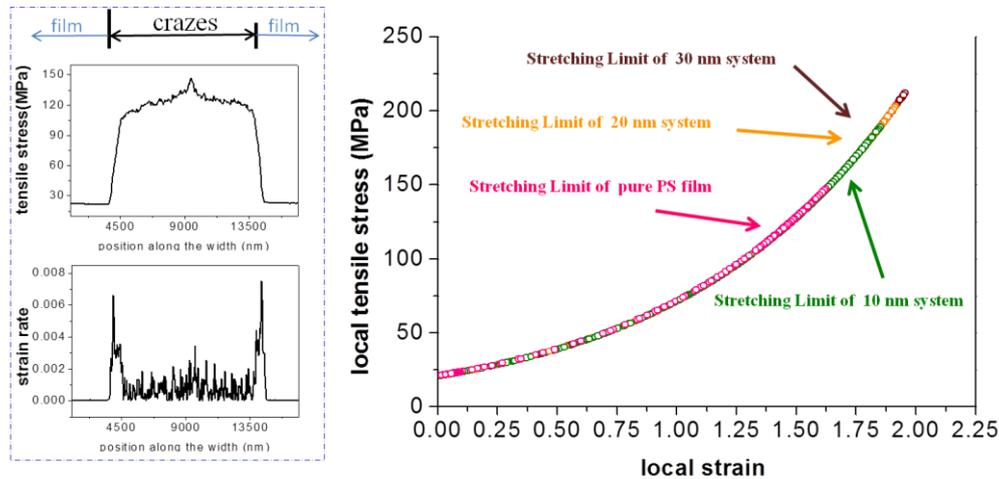
Figure 11. Profiles of the local stress and strain rate within the craze along the stretching direction. Also shown is the inter-relationship between the local stress and strain for the neck drawing for various samples, of which the detailed data are shown in Fig. 12.

8
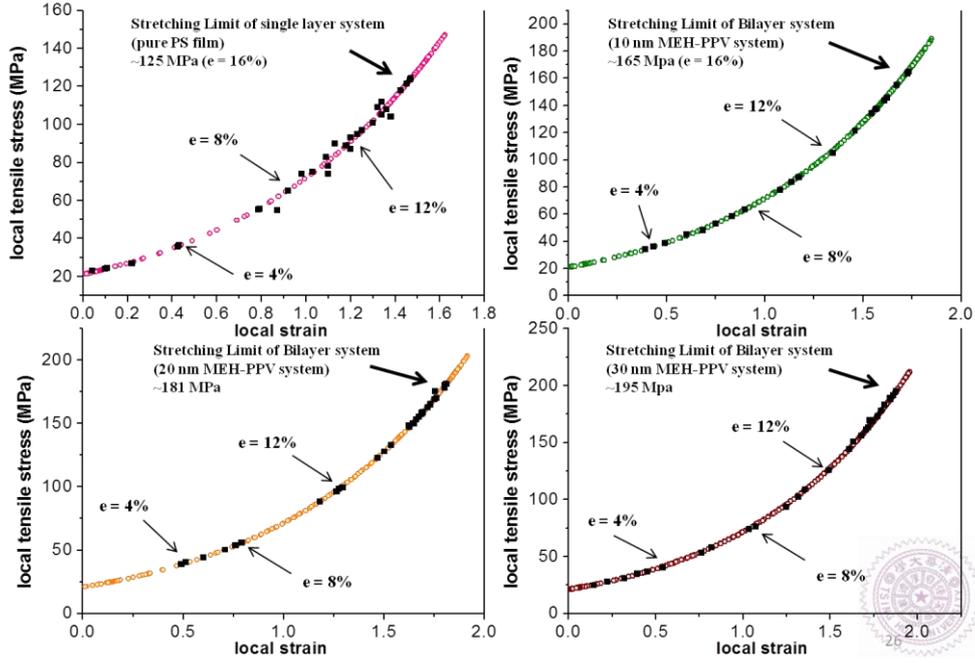
Figure 12. The local stress versus strain for craze formation in the various samples.

The PL emission of the stretched bilayer films was found enhanced dramatically. For only 15% stretched volume fraction in the bilayer films, the PL intensity increased 2.4 fold, 1.75 fold, and 1.40 fold respectively for the 10 nm, 20 nm and 30 nm MEH-PPV films (Fig. 13). The PL enhancement of the whole film, γ, can be related to both the local PL enhancement in the local deformation zones ($\xi_c = i_c/i_{f,0}$) and that outside the local deformation zones ($\xi_f = i_{f,c}/i_{f,0}$) as

$$\gamma \equiv \frac{I_t}{I_{t,0}} = \left(\frac{i_{f,c}}{i_{f,0}}\right)\frac{(1-e+e_c)}{1+e} + \left(\frac{i_c}{i_{f,0}}\right)\frac{e-e_c}{(\varepsilon+1)(1+e)},$$

which can be simplified as

$$\gamma(1+e) = \xi_f + \left(\frac{\xi_c}{\varepsilon+1} - \xi_f\right)(e-e_c)$$

where I_t is the total PL intensity, $i_{f,0}$ is the specific PL intensity of the film before stretching, $i_{f,c}$ is the specific local PL intensity of the regions outside the crazes, i_c is the specific PL intensity in the crazes, and λ_c is the draw ratio of the crazes.

9
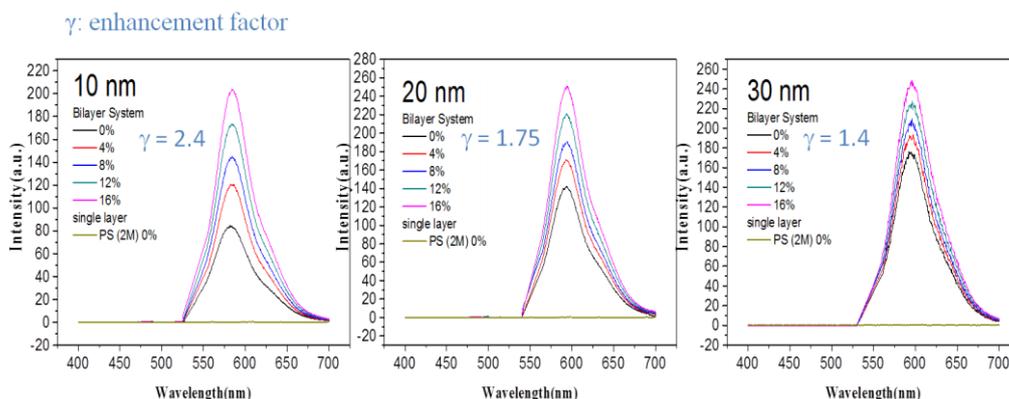
Figure 13. The PL spectra of the MEH-PPV layers for various applied strain in the bilayer films.
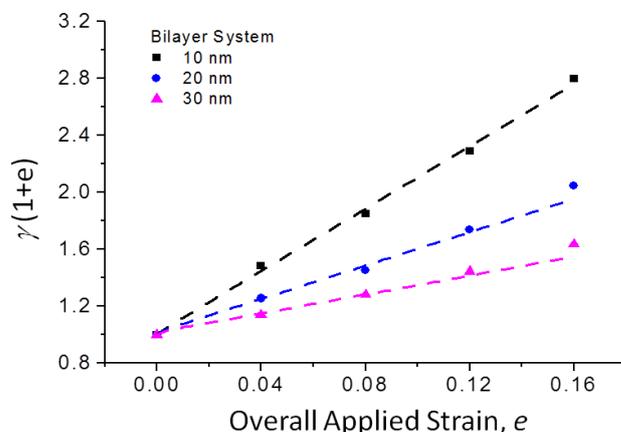
Figure 14. The plot of the bilayer PL enhancement γ multiplied with the overall draw ratio $(1+ e)$ of the bilayer versus the applied strain e to the bilayer films yield the local PL enhancements of the crazes ξ_c and of the regions outside the crazes ξ_f, as derived in the text.

The local PL enhancement in the crazes of the neat MEH-PPV was found to be as high as 48 fold, smaller than but still comparable to those observed, ranging from 50 to 70 fold, for the diluted MEH-PPV in optically inert PS matrix. Evidently, when the conjugated macromolecules are effectively stretched, the PL efficiency of the neat resin still increases similarly to that observed before for the stretched diluted systems. As the thickness of MEH-PPV film increased, the enhancement decreased along with the decrease of local stresses. A plot of all the data of ξ_c and ξ_f for the various MEH-PPV thicknesses clearly indicates the good correlation between the PL enhancement and the applied mechanical stress. Therefore, we can conclude that tensile stresses may give rise to great enhancement in the optoelectronic efficiencies of high concentration polymers as long as the mechanical deformations are down to the molecular level.
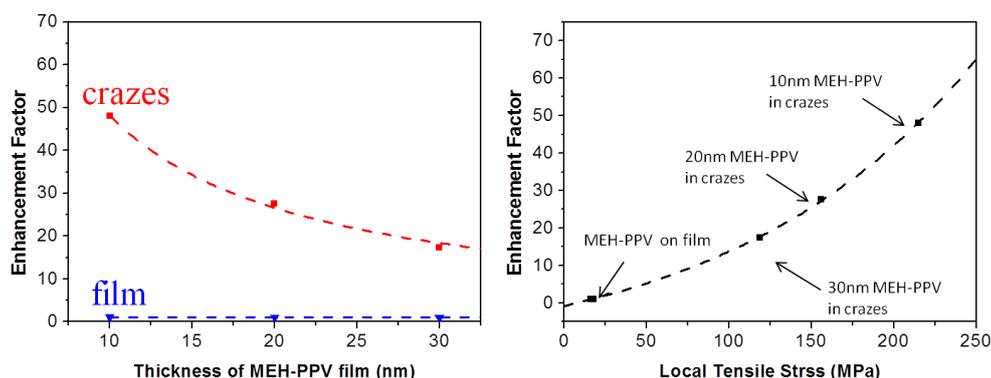
Figure 15. The PL enhancement factors ξ_c and ξ_f for various MEH-PPV thicknesses and the correlation of these PL enhancements with the determined local stresses.

The details of the molecular scale deformations responsible for the enhancement of the PL efficiencies were probed further with confocal PL spectroscopy. Due to the difference detector used in the micro-PL spectrometer, the PL spectra varied slightly relative to those obtained using the regular PL spectrometer (Horiba Jobin Yvon Fluorolog-3). The micro-PL spectra (probed with a beam size of ~ 1μm) from local spots outside the crazes and within the crazes (Fig. 16) for the various MEH-PPV layer thicknesses were shown in Fig. 17. Note that the PL intensity detected by the confocal micro-PL spectrometer was strongly influenced by a form factor waveguide effect of the craze microstructure due to the beam path geometry. Hence the PL intensity obtained by the confocal micro-PL cannot be used to determine the actual PL enhancements. The wavelengths of the PL peaks, however, can be used to reveal important information associated with the molecular deformations in the crazes that resulted in the massive PL enhancements.
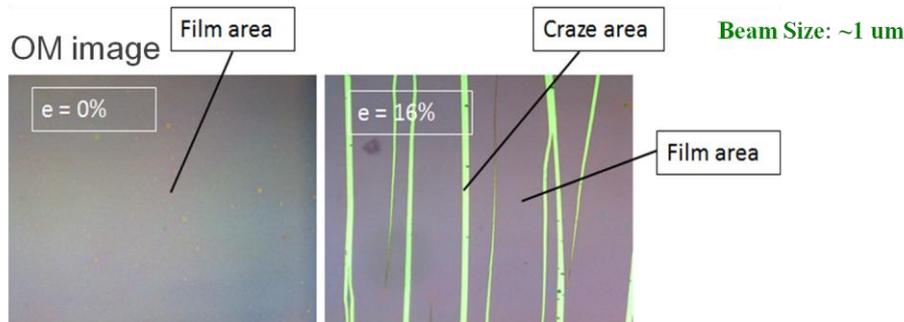
Figure 16. With the probing beam size of around 1 μm, the local emission behavior of the conjugated polymer MEH-PPV before and after the mechanical stretching can be determined as a function of position of varied local stress and strain.

Clearly, as shown in Fig. 17, a new blue-shifted peak at ~555 nm was arising at the expense of the original intermolecular emission peak at 586 nm as the mechanical deformation increased. The new peak increased in intensity but the emission wavelength was unchanged as the applied strain increased, which is fully understandable in view of the increase of the total plastic deformed macromolecules in the crazes where the local stress and strain were roughly the same. However, as the stress increased when the MEH-PPV layer thickness decreased, the new peak still remained approximately unchanged at the same wavelength of ~555nm with the spectral shape evolved into one that was highly domnated by the blue-shifted new peak. It is important to note that the small fractions of stretched

11

MEH-PPV molecules in the sample (less than ~1.5 wt.%) had masked the observation of this blue shift in the PL spectra obtained for the whole samples.

This new peak at ~555 nm was almost identical to that in the PL spectra of the highly diluted MEH-PPV films where the peak position was not altered by stretching in the single layer drawing (Fig. 18). Therefore, it is believed that the blue shift was due to separation of the molecular aggregates in the neat MEH-PPV film and the new peak was that corresponding to the luminescence where molecular aggregates were absent, such as that in the very diluted systems. It remaining intriguing that the stretching of the "single molecules" in the diluted system did not produce transient molecular kinks as observed in the dewetting of ultrathin films. The scale of the deformation, as limited here by the spacing of the craze fibril spacing, may contribute to this behavior.
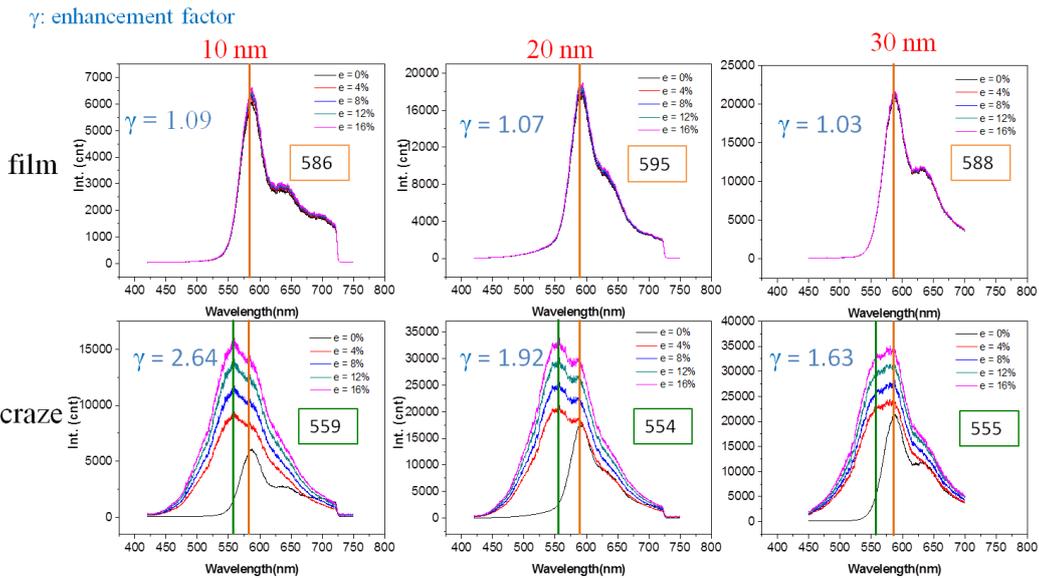
Figure 17. The micro-PL spectra obtained from probing of the local spots outside the crazes and within the crazes for the various MEH-PPV layer thicknesses. Note that the PL intensity was strongly influenced by a form factor waveguide effect of the craze microstructure and hence cannot be used to evaluate the actual PL enhancements. Only the wavelengths of the PL peaks were considered and discussed here.
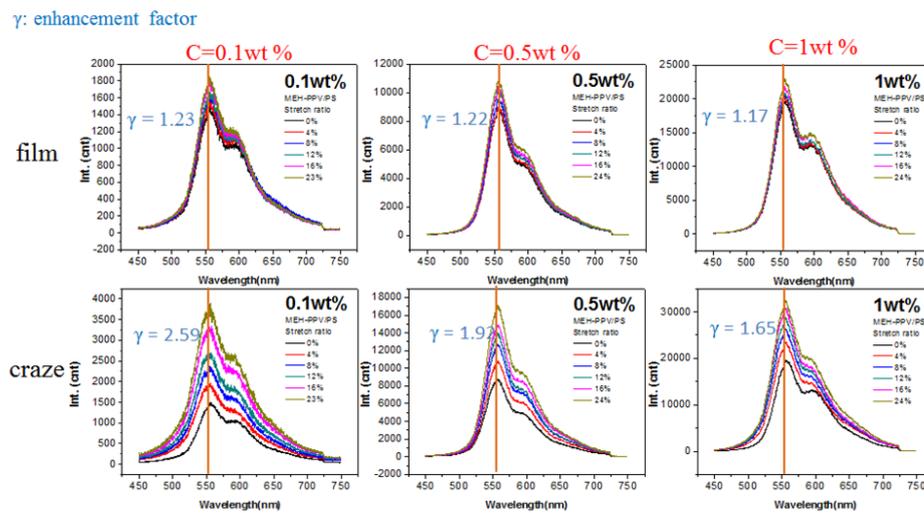
Figure 18. The confocal PL spectra of diluted MEH-PPV (concentration = 0.1wt.%, 0.5 wt.%,

12

and 1.0 wt.%) in PS stretched for various applied strain e's in single layer films.

C. **Ultrafast (Sub-Pico Seconds) Experiments**
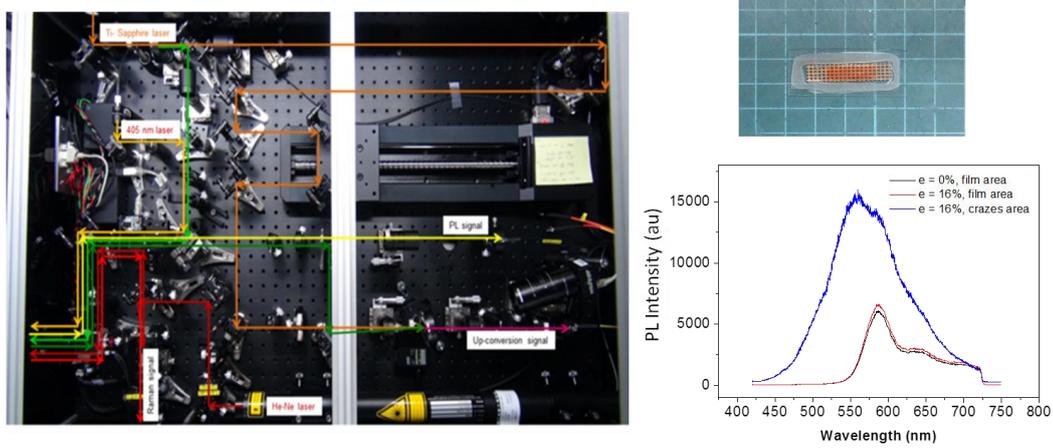
Figure 19. The up-conversion femto-second time-resolved AFM-integrated micro-PL spectrometer, the packaged samples to prevent oxidative degradation during the probing, and the calibration spectra of the samples.
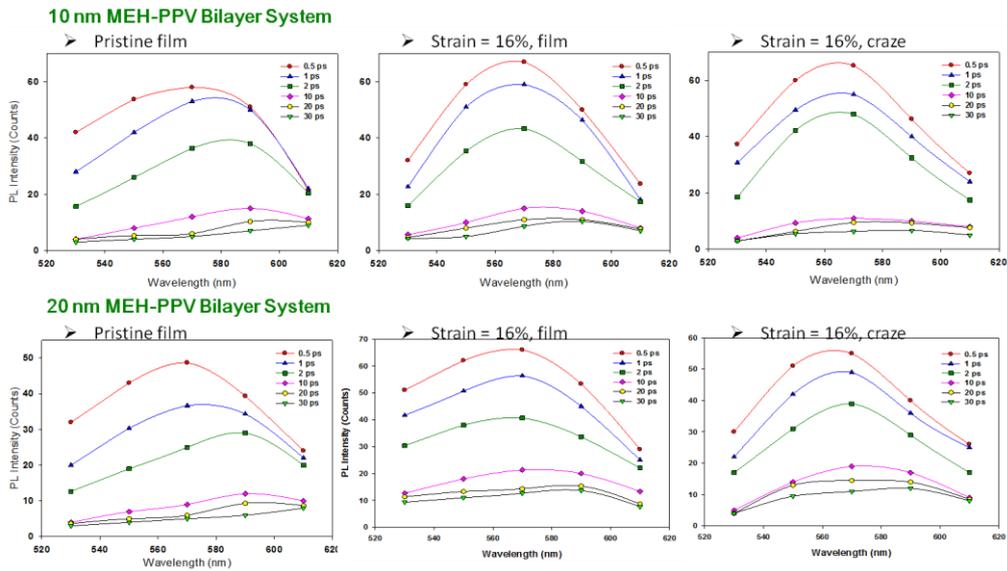
Figure 20. The PL spectra of the MEH-PPV films (10 nm and 20 nm) before and after stretching (from inside the crazes and outside).
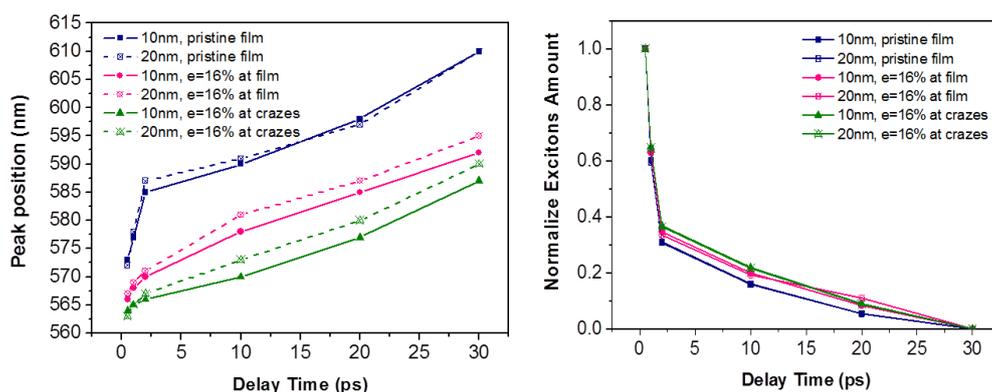
Figure 21. The peak of the time-resolved PL of the MEH-PPV before and after the stretching (within and outside the crazes); and the normalized decay of recombined excitons as a function of the delay time after the pulse excitation.

The bilayer films, after insulation packing, were further studied in the confocal optical system using the up-conversion femtosecond laser for sub-picosecond time resolved PL analysis. The PL spectra of the MEH-PPV films (10 nm and 20 nm) before and after stretching (from inside the crazes and outside) were shown in Fig. 20. It was found that the PL emission generally underwent a red shift as the delay time (after the excitation pulse) increased. For the pristine film before stretching, the red-shift rate was almost the same in both systems of 10 and 20 nm (Figure 21). The red shift, however, was substantially slowed when the conjugated polymer was stretched, particularly in the time regime less than 2ps (Fig. 21). The fractional decay of the PL intensity (the number of recombined excitons) as a function of the delay time, however, was not changed by the mechanical stretching.

It may be concluded here that the massive enhancements of the PL efficiencies is correlated with the energy transfer process in the conjugated polymer chains right after absorption of photons, particularly in the time frame of less than 2ps. This newly observed correlation is consistent with the depression of the electron-phonon coupling in the stretched polymer chains that may cause a decrease of exciton trapping and hence the increase of the optoelectronic efficiencies.

C. Stretching the Neat Polythiophene Films:

Following the same methodology, the conjugated polymers of thiophene backbone but with varied side chain length for controlled intermolecular interactions (P3EHT, P3BT, and P3HT) were stretched in the bilayer structure supported by a PS film ($\tau = 0.5$ μm). The molecular weights of the thiophene polymers were 30kg/mol., 50kg/mol., and 50kg/mol. for P3EHT, P3BT, and P3HT, respectively.

All three polythiophene polymers developed well-defined local deformation zones (Figs. 22-24) similar to the crazes in the single layer PS.

The effect of the mechanical stretching on the PL behavior of these stretched films, however, was strongly dependent on the side groups (Fig. 25). With the bulkiest side group, the P3EHT demonstrated some PL enhancements in the order of 15 fold within the crazes. The enhancement of the PL efficiency quickly diminished as the intermolecular interactions strengthened by the reduced bulkiness of the side group. For P3HT and P3BT, the PL enhancements were negligible and comparable to each other, indicating that the bulkiness rather than the linear length counted for blocking the intermolecular interactions.

It may also be concluded that interactions may prevent the effect of mechanical stress to

14

be realized when they become strong enough to foster the formation of molecular aggregates. According to the polaron theory, exciton trapping in the 1D system is lightly trapped while for 2D and 3D systems exciton trapping are deep trapped. The formation of molecular aggregates is likely to create the 2D or 3D deep-trap landscape for excitons, hence leading to ineffectiveness of the mechanical stretching effect.
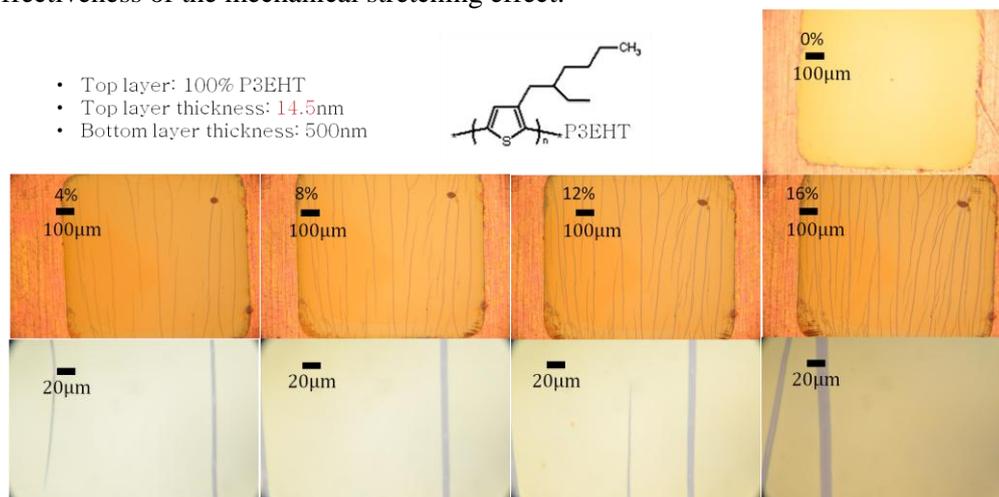
Figure 22. The thin layer of neat P3EHT (τ =14.5 nm) was stretched on the PS film (τ = 0.5 mm) that was bonded to a piece of ductile copper grids for non-relaxed deformations.
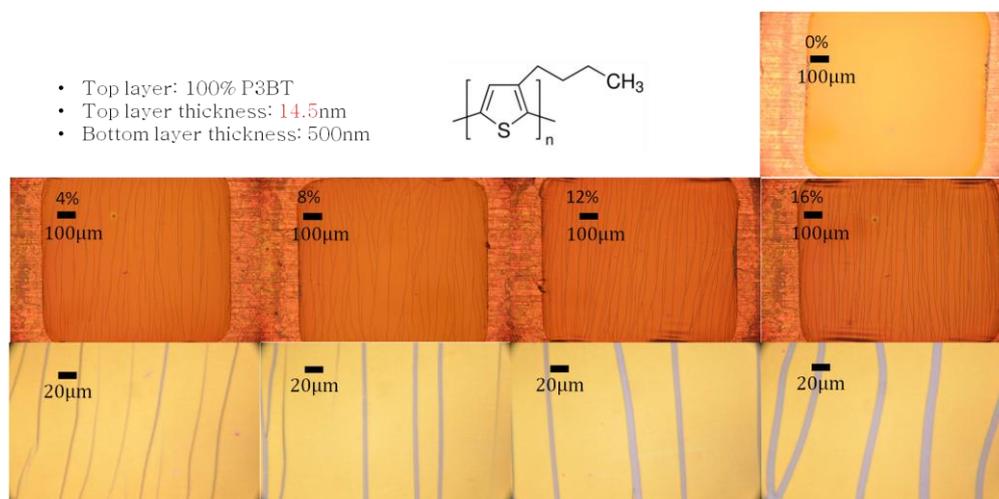
Figure 23. The thin layer of neat P3BT (τ =14.5 nm) was stretched on the PS film (τ = 0.5 mm) that was bonded to a piece of ductile copper grids for non-relaxed deformations.
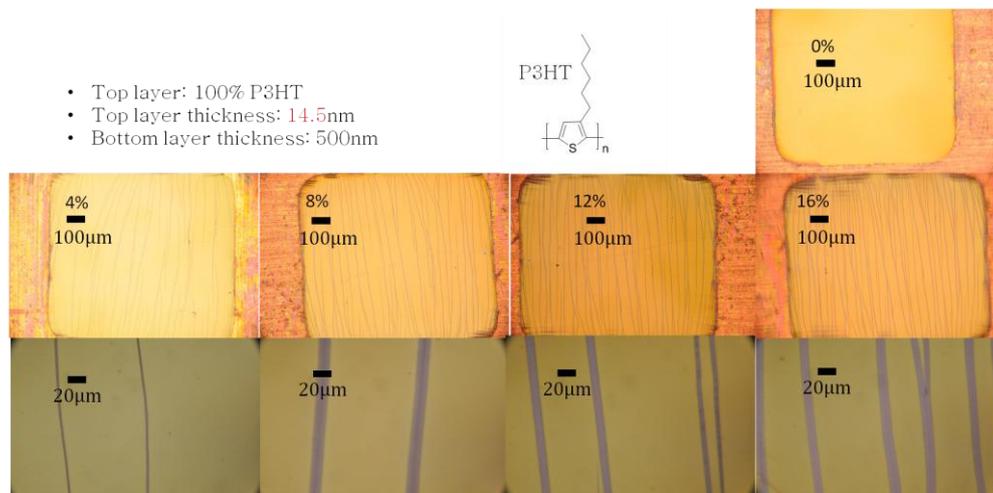
Figure 24. The thin layer of neat P3HT (τ=14.5 nm) was stretched on the PS film (τ = 0.5 mm) that was bonded to a piece of ductile copper grids for non-relaxed deformations.
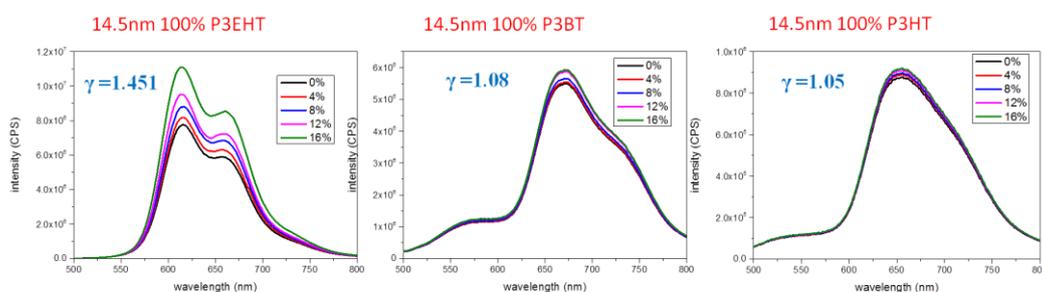
Figure 25. The PL spectra of the three thiophene polymers as a function of stretching.

2. Imprinting Conjugated Polymer Films

The imprinting method was explored for its feasibility for imparting the stress-induced efficiency enhancements to the manufacturing of optoelectronic devices based on conjugated polymers. The sample of a thin polymer film of PS containing an amount of the conjugated polymer (MEH-PPV or P3HT) was prepared by spin-coating on glass slide where the heterojunction quenching effect was absent such that the changes of PL emission was only due to molecular deformations and not the height changes.

It was found that imprinting on thinner films, owing to the substrate effect, resulted in deeper footprints. Generally, polymer films of a thickness in the vicinity of 50 nm, which is comparable to those used for optoelectronic devices, produced good printing results. Molds of two feature sizes, nominally 5.0 and 0.5 μm, were used (Fig. 26). Imprinting tests were carried out at room temperature as well as 100C. The imprinting stress was fixed and the imprinting depth increased with the imprinting stress in the range between 200 and 800 MPa.

Although imprinting at the higher temperature of 100C produced better footprints, no PL enhancements were observed as a result of the imprinting, likely due to the diminishing stresses in the imprinted conjugated polymer during and after the imprinting. Imprinting at the room temperature usually produced small footprints (Fig. 27), particularly when the larger mold (5 μm feature size) was used.

For MEH-PPV, imprinting using the small mold (0.5 μm feature size) may produce

16

small PL enhancements when the MEH-PPV concentration in the PS film was dilute and the enhancement vanished completely as the MEH-PPV concentration became greater than 20 wt.% (Fig. 28). While a contact time of 20 minutes was generally used for the imprinting, the PL spectra were found to be independent of the contact time from 30 seconds to 12 hrs. The lack of PL enhancement is attributed to the effective relaxation of imprinting stress after de-molding.

For P3HT, a small PL enhancement due to imprinting was observed even at low P3HT concentration (at 5 wt.%, e.g.), as shown in Fig. 28. The PL enhancement was found to increase as the P3HT concentration increased, in contrary to what observed for MEH-PPV. The PL enhancement, however, was later found to be dependent on the contact time at imprinting and hence was attributed to stress-induced re-crystallization that may stiffen the polymer chains and produce the effect of suppressing the electron-phonon coupling.

Further experiments were ongoing on the deformation scales down to the nanometer range.

5-μm mold

0.5-μm mold
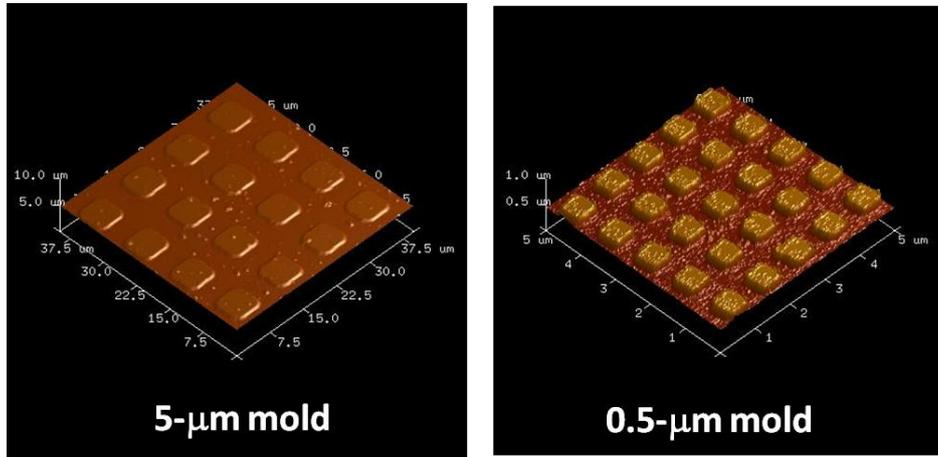
Figure 26. The molds (5-micron size and 0.5 micron size).

10% MEH-PPV 600MPa 0.5um mold imprint at room tempertaure

10% MEH-PPV 600MPa 0.5um mold imprint at room temperature

10% P3HT 600MPa 0.5um mold
imprint at room temperature

10% P3HT 600MPa 0.5um mold
imprint at room temperature
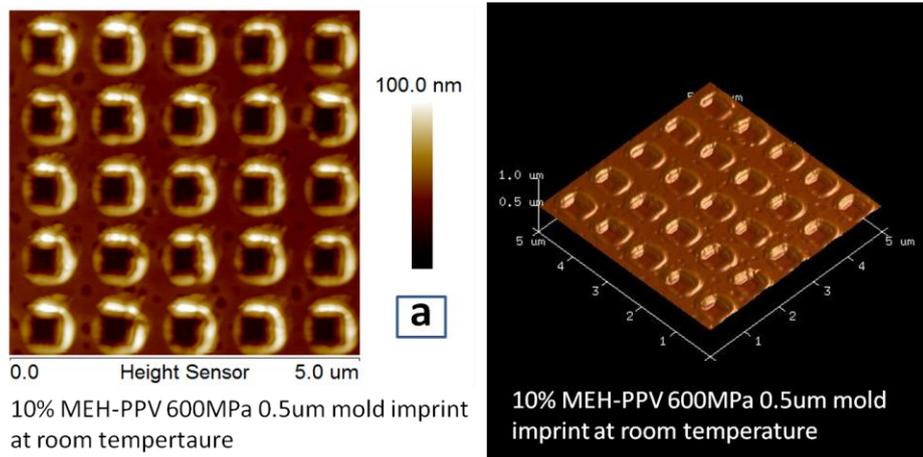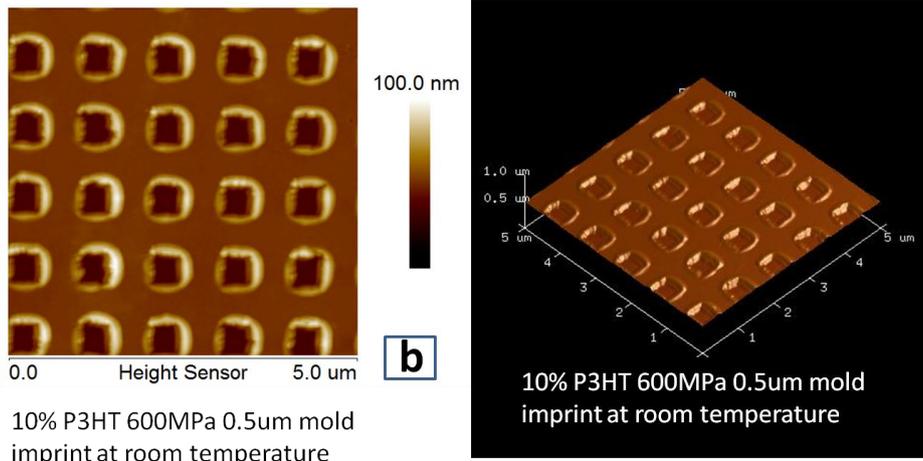
Figure 27. The imprint footprints of the MEH-PPV and P3HT samples (50 nm) with concentration of 10 wt.% in PS.
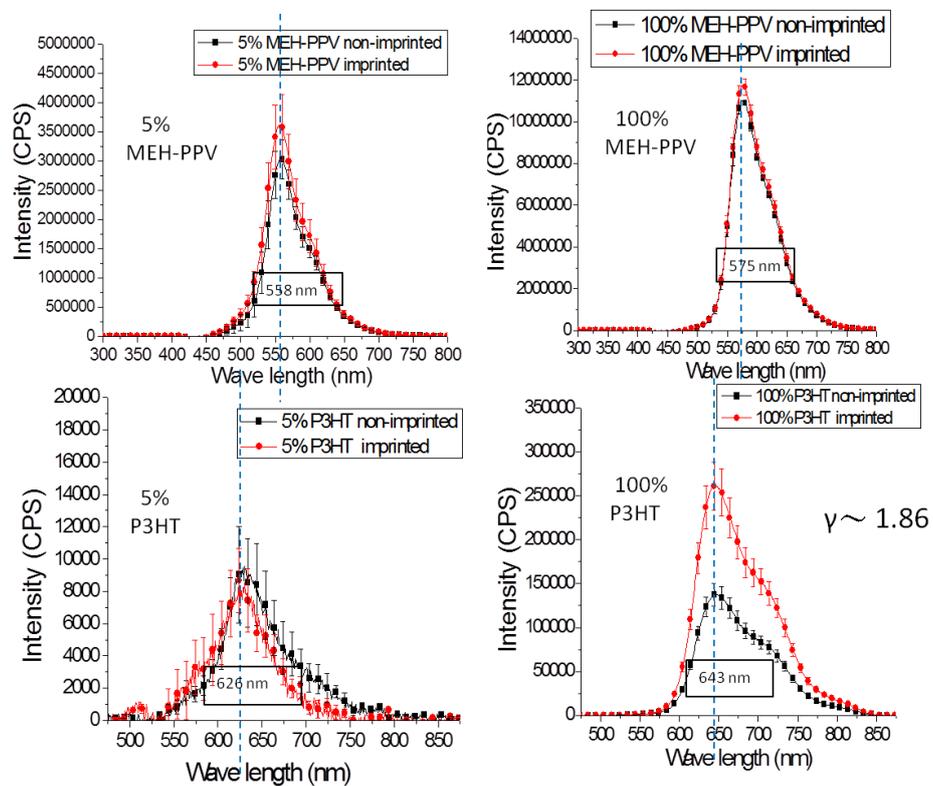
Figure 28. The PL spectra of the imprinted conjugated polymer samples.
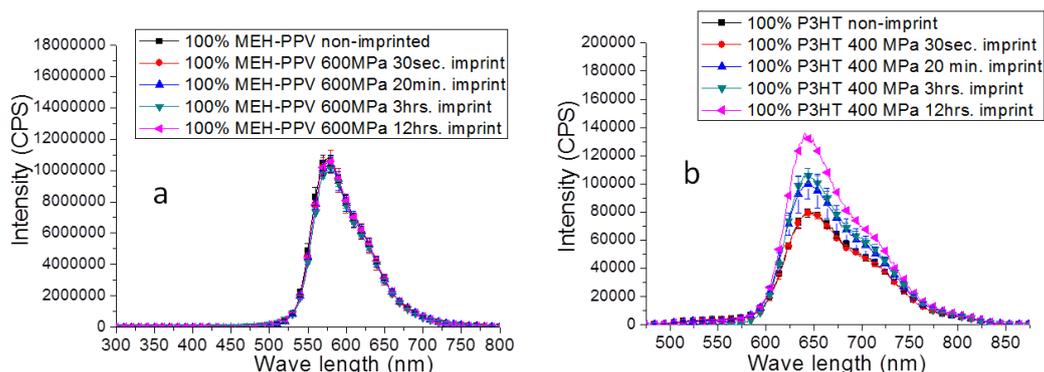
Figure 29. The PL spectra of the neat MEH-PPV and P3HT as a function of the contact time for imprinting before demolding.

3. The Reciprocal Mechano-Optical Effect: Light-Induced Mechanical Changes

A corollary of the stress-induced enhancement of optoelectronic efficiency is the existence of light-induced changes of molecular mechanics of the conjugated polymer chains.

This anticipated behavior was indeed observed in the dewetting of thin conjugated polymer films annealed at elevated temperature. When illuminated under the light of the energy falling in the absorption range of the conjugated polymer, the polymer chain mobility decreased dramatically and the dewetting was effectively stopped even at the elevated temperature.

We went further to manipulate the conjugated polymer MEH-PPV chains with the light letting through an optical mask when the polymer chains were plasticized in a good solvent vapor (Fig. 30). We found that the polymer chains can be patterned according to the mask although they behaved differently from that during thermal annealing due to the existence of the solvent molecules. In addition, the molecular flows induced by lighting were reversed as the conjugated molecular concentration went from the dilute regime to the concentrated. The unique light-controlled mechanical behavior is explained by the conformation changes of the conjugated polymer upon photon absorption which in turn caused changes of solvent sorption resulting in the directed movements of the macromolecules.
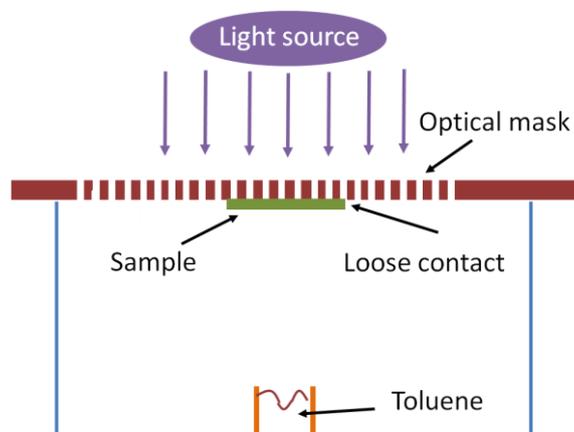
Figure 30. A thin polymer film composed of MEH-PPV and PS molecules were exposed to toluene vapor while it was shine with patterned light through an optical mask.

Firstly, for samples of low MEH-PPV concentrations, the lighted regions under the mask increased in thickness during the solvent annealing process, gradually forming ridges with the final height to be around 70 nm for a 30 nm film of 15 wt.% MEH-PPV, exposed under the 5 μm (feature size)-mask. The ridges in increase in height approximately linearly with the annealing time at the beginning (growth rate ~3nm/min. for the 10 wt.% MEH-PPV sample) until it saturate. In contrast, the regions without light exposure were receding, ultimately down to a thickness below 3 nm. By this way, the pattern on the mask may be transferred to the polymer film (Figs. 31-33). Clearly, net polymer flows occurred from the dark regions to the lighted regions. This "residual layer" of ~ < 3 nm created in the dark regions was very similar, in both the thickness and formation mechanism, to those commonly observed in thin film dewetting. Hence, capillary forces are believed also had participated in the molecular flows directed by the shining light.
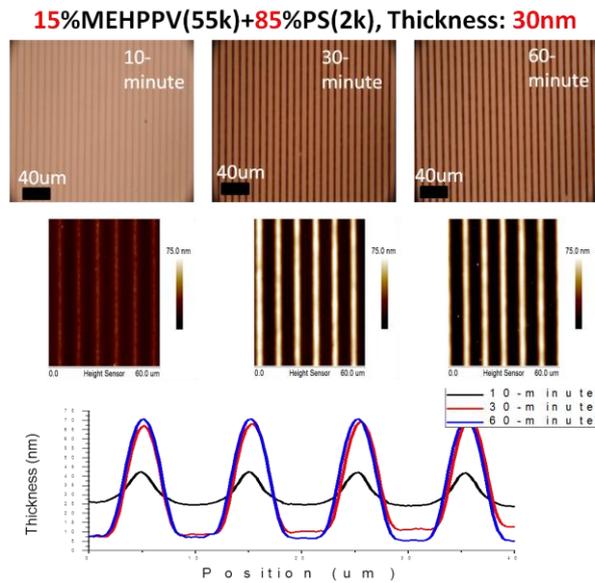
Figure 31. Patterning the MEH-PPV molecules in a 30 nm film (15 wt.% in PS) under the light exposure through the 5-micron optical mask.
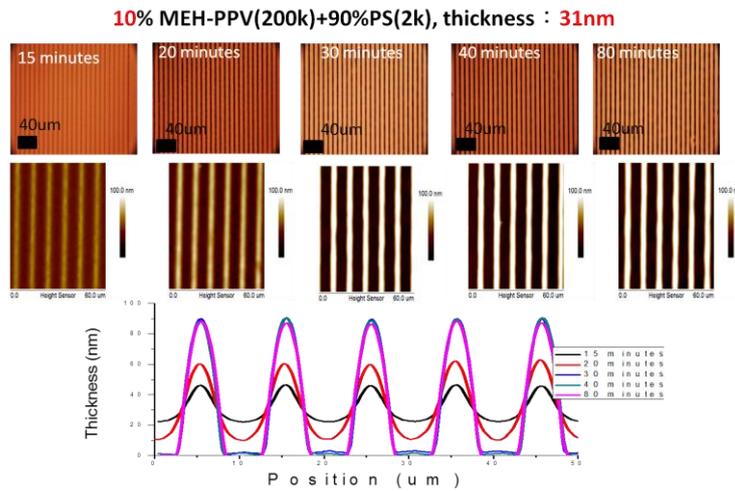
Figure 32. Patterning the MEH-PPV molecules in a 30 nm film (10 wt.% in PS) under the light exposure through the 5-micron optical mask.
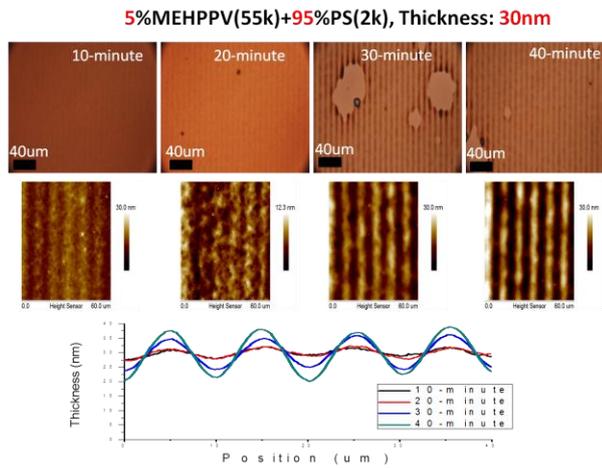
Figure 33. Patterning the MEH-PPV molecules in a 30 nm film (5 wt.% in PS) under the light exposure through the 5-micron optical mask.
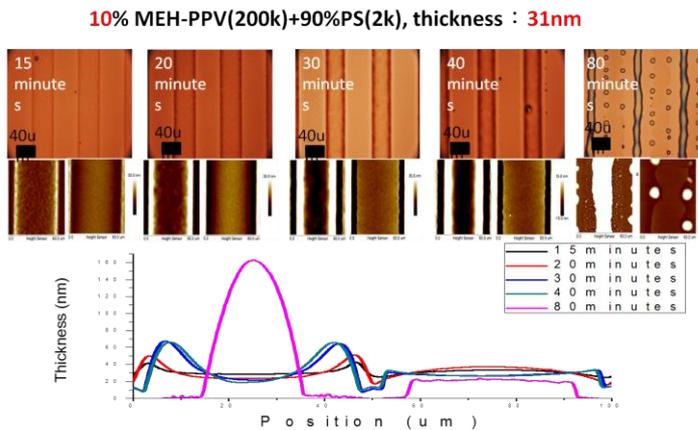
Figure 34. Topographic profiles crossing the lighted and dark regions as a function of solvent annealing time for a 30nm film of 10wt.% MEH-PPV in PS under the 50 μm mask.

5%MEHPPV(200k)+95%PS(2k), Thickness: 30nm
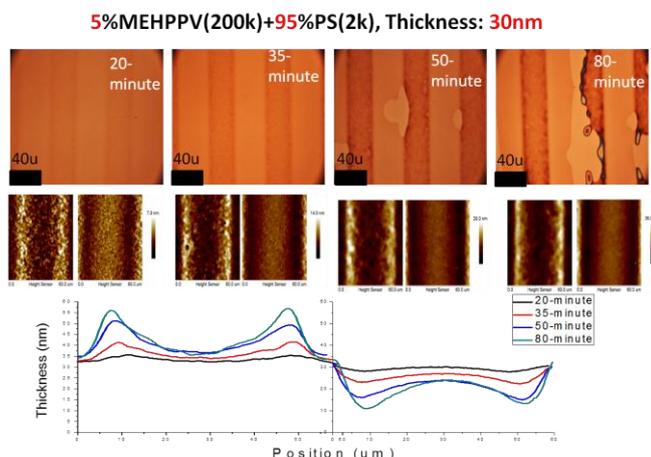
Figure 35. Topographic profiles crossing the lighted and dark regions as a function of solvent annealing time for a 30nm film of 5 wt.% MEH-PPV in PS under the 50 μm mask.

For larger feature sizes of the mask (e.g. 50 μm), similar macromolecular flows also occurred, forming ridges that first emerged at the edges of the lighted areas, then moved, while growing in height, toward the center of the lighted regions, and later on coalesced to form a central ridge with a final height reaching ~180 nm (for 30 nm film of 10wt.% MEH-PPV) under the 50 μm mask (Fig. 34). In the dark regions, on the other hand, receding took place first locally at the interface between the dark and lighted regions (Fig. 35) when the rest of the area remained unchanged. As the solvent annealing went on, while the dark regions maintained a approximately flat surface with the thickness decreasing slowly, the local receded regions at the interface deepened and expanded laterally in the both directions with the advancing front moving faster toward the light regions. When the receding area eventually evolved into the "residual layer" of below ~3nm, the lateral fronts may encompass a swatch of a region with width of ~20 μm dotted with polymer droplets left behind the dewetting fronts. Note that in the case of 5 μm mask exposure, no droplets were observed when the dark regions evolved into the residual layer.

In this dilute concentration regime, the ridge height and the receding depth decreased with reduced MEH-PPV concentration. The flow rate, on the other hand, increased concomitantly (Figs. 33, 35).

The driving force for the molecular flows is the diffusion of the mobile PS chains toward the regions where the local entropy had decreased due to backbone straightening of the MEH-PPV molecules under the light exposure.

22
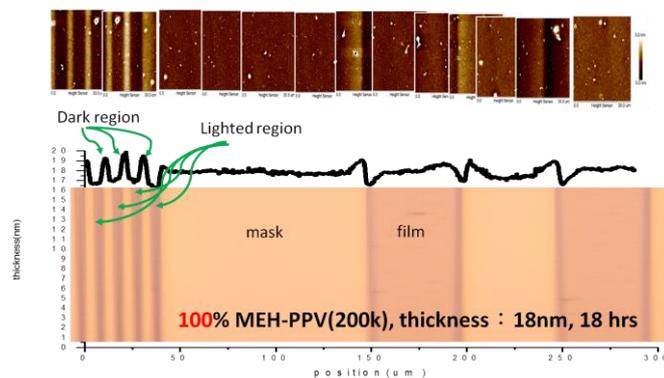
Figure 36. Topographic profiles across the lighted and dark regions for neat MEH-PPV film (18 nm) under the mask of both the 5 μm and 50 μm features.
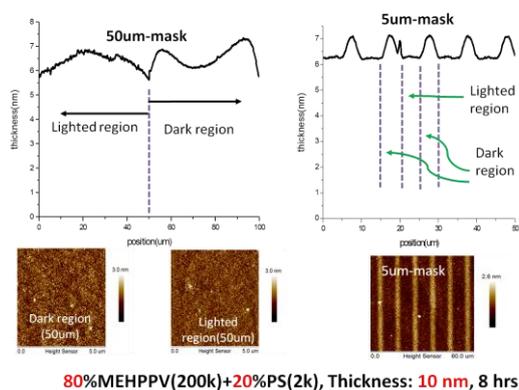
Figure 37. Topographic profiles of the lighted and dark regions for the film containing 80% MEH-PPV in PS (10 nm) exposed under both the 5 μm and 50 μm masks.

For higher concentrations, the molecular flows slowed substantially and the directions reversed (Figs. 36, 37, 38) in that the local thickness in the dark areas increased with solvent annealing while the lighted areas underwent a process similar to the receding but the "residual layer" state was never attained (Fig. 37). The reverse in the flow direction was due to the absence or insufficiency of the mobile PS molecules in the soaked film where the molecular flows were enacted mainly by the movement of the conjugated polymer that tended to diffuse into the dark regions in order to increase the overall entropy, i.e., to increase the total free energy. The flows of the light-rigidified MEH-PPV molecular chains was very slow, taking ~18 hrs to create a ridge height of ~3 nm (for the 100% MEH-PPV, Fig. 36) that would have been taken approximately 1 min. by the mobile PS flows to achieve the same height. Hence, although the driving force for the light-rigidified MEH-PPV flows still existed in the low concentration samples while the samples were solvent annealed and exposed under the mask, the flows were too slow such that the mobile PS movements effectively swamped their emergence.

23
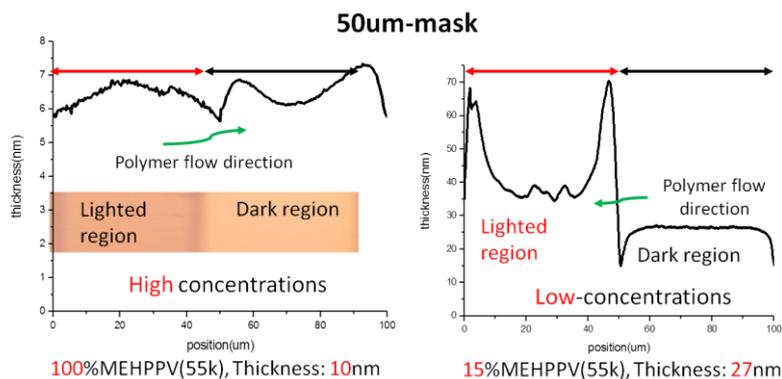
Figure 38. Analysis of the molecular flows across the lighted and dark regions (under the 50 μm mask) for the low and high MEH-PPV concentrations.

The molecular flows resulted in not only the topographic patterns on the polymer films, but also imparted changes to the PL emission behavior of the conjugated polymer chains. As probed by using the confocal micro-PL spectrometer, the lighted regions of a low MEH-PPV concentration exhibited remarkable blue shifts (Figs. 39, 40), consistent with the chain separation effect arising from the in-flows of the mobile PS chains. At the dark regions where the film eventually evolved into the residual layer, the PL spectrum also underwent blue shift to ~543 nm and the intensity was enhanced considerably. This observation is consistent with the effects of molecular flows triggered by thin film dewetting.

The results presented here clearly illustrate the reciprocal effect of the stress-induced PL enhancements, not only further providing solid evidence for the existence of the mechanical effect but also shed some light for manipulation of the conjugated polymers using a dramatically different approach by selected-area light exposure methods.
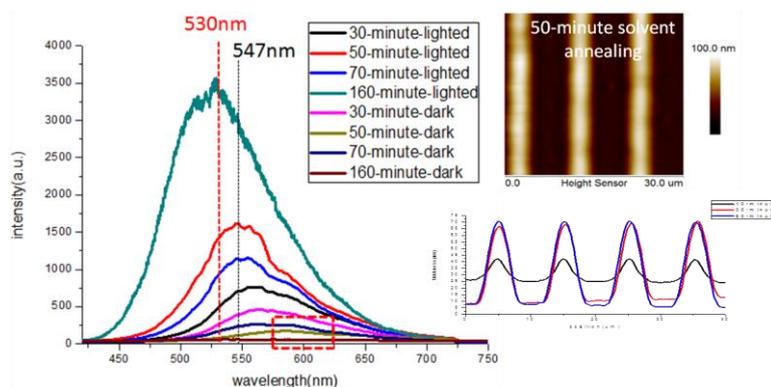
Figure 39. The PL spectra obtained using the confocal micro-PL spectrometer from the local spots of the patterned film via solvent annealing under masked light exposure.
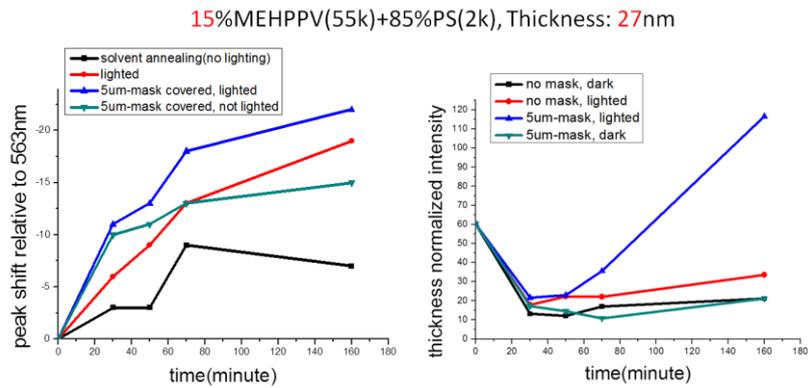
Figure 40. The emission peaks and the thickness-normalized PL intensity of the PL emission from the various spots of the patterned films.

4. Electro-Poling of Conjugated Polymers Thin Films

Mechanical stretching of conjugated polymer chains has been shown clearly to have the effect for producing massive enhancements of the optoelectronic efficiencies. Hence, finding the suitable methods that can impart effective mechanical stresses and strains to the conjugated polymers and concomitantly are compatible with the mainstream manufacturing processes obviously appears to be one of the next logical targets for useful research. It is well known that a strong electric field may polarize and orient molecular segments (poling) to impart molecular strain and stress. Electric poling may be less susceptible, compared to the externally applied mechanical deformations, to the blocking effect of molecular aggregatesas to impart the mechanical stress effect because electric field can penetrate the polymer solid and enforce segmental stretching down to the proper molecular scales. It is also compatible with the processing methods for optoelectronic or microelectronic devices. In addition, new information regarding the molecular movements, packing states, and the optoelectronic behavior may be gained from such explorations.
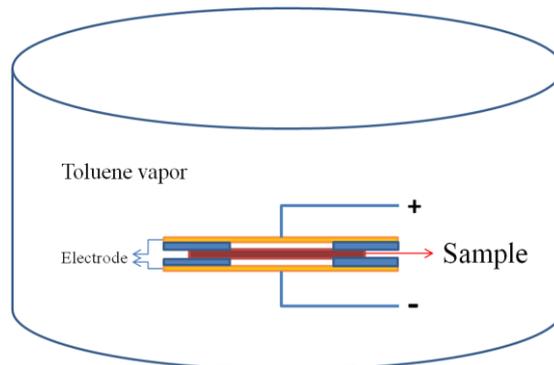
Figure 41. A schematic depiction of the electropoling experiment.

For the experiment, the conjugated polymers MEH-PPV and P3HT (r.r. ratio = 95%, r.r. ratio = 50%) with the molecular weights 200kg/mol. (MEH-PV), 35 kg/mol. (P3HT, rr = 95%), and 10 kg/mol. (P3HT, rr ratio = 50%) were studied. An optically inert polymer, polystyrene (PS, M=2kg/mol.), was used to blend with the conjugated polymer for

25

controlling the molecular packing and chain mobility. Thin films of the conjugated polymers (or their blends with PS) were prepared by spin coating from the solutions on glass slide. The film on the substrate was then clamped between electrodes with insulating spacers and poled under a high voltage of ~4 kV in an enclosed chamber (Fig. 41) where toluene vapor was permeating so that the polymer chains were plasticized and responsive to the poling. After poling, the PL spectrum was taken while the conjugated polymer chain orientation was probed by x-ray absorption spectroscopy.
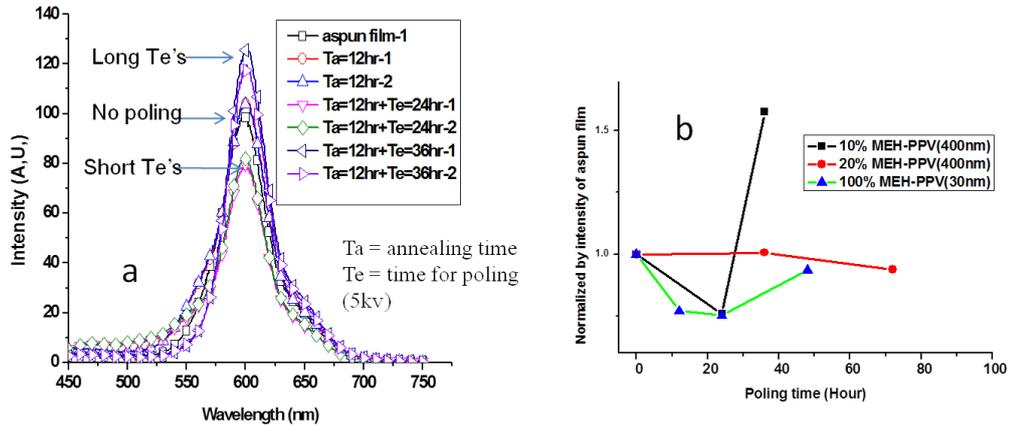
Figure 42. (a) PL spectra of the 10wt.% MEH-PPV samples during poling. (b) The PL intensity changes during poling (PL=1 for initial film before poling).

For the non-crystalline MEH-PPV which, however, may form molecular aggregates, the poling was found to produce several significant effects. From AFM inspection, large-scale cooperative molecular movements of the conjugated polymer occurred during the poling. On the segmental scale, polarization took place to give rise to variations in the photoluminescence. For samples of MEH-PPV low concentration (< 15 wt.% in PS), the emission peak did not shift with poling and the PL intensity first decreased (exciton separation by electret) and then increased, consistent with stress-induced efficiency enhancement (Fig. 42). For the higher concentrations (>15 wt.%), a red shift was observed along with the small PL decrease at the beginning of the poling, which was attributed to the solvent-induced formation of molecular aggregates. Continuous poling caused the PL to increase modestly (Fig. 43).
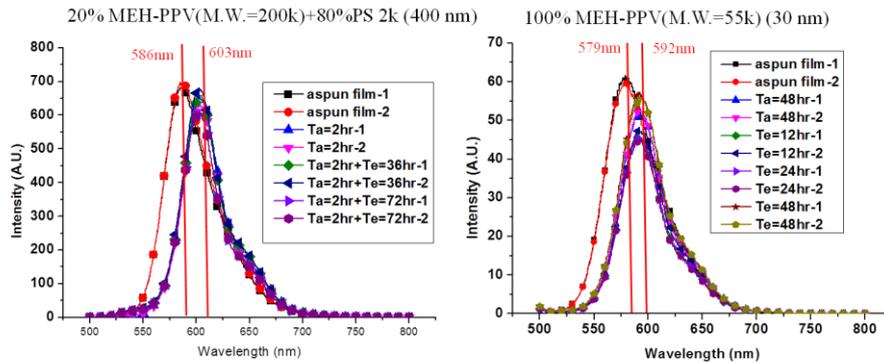
Figure 43. PL spectra of the high-concentration samples of MEH-PPV poled as a function of time in solvent vapor.
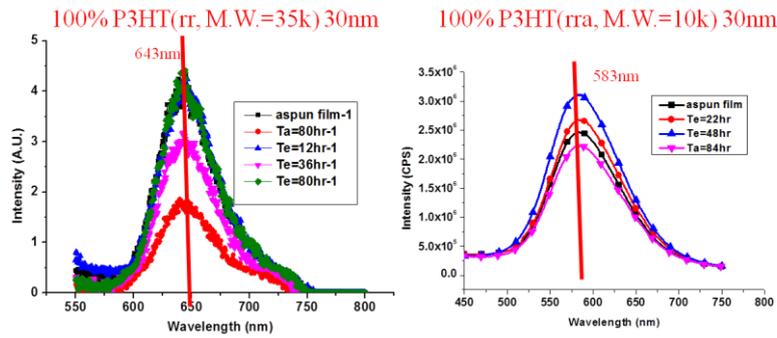
Figure 44. The PL spectra of P3HT as a function of poling for both the regioregular and the regiorandom P3HT.
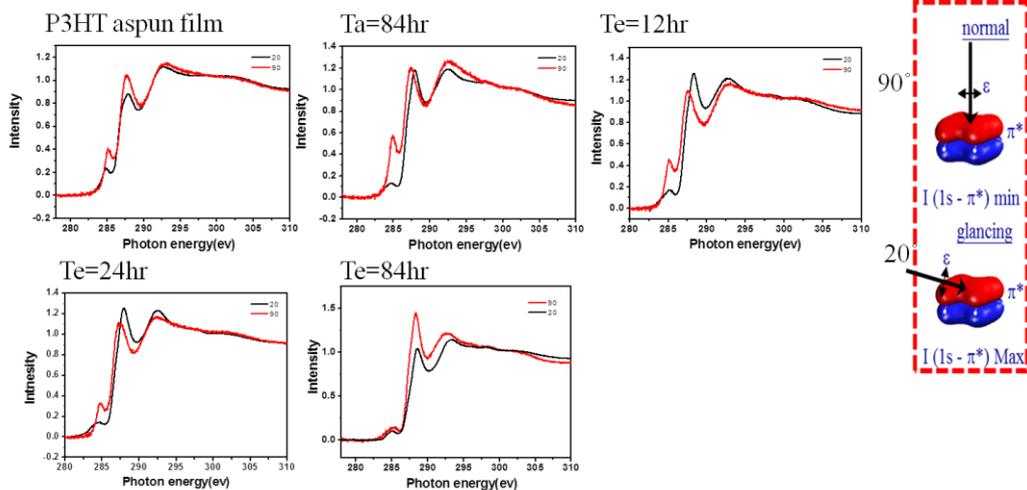
Figure 45. The x-ray absorption spectroscopy of the poled P3HT samples.

For the P3HT polymers, the PL spectra did not exhibit any shift versus the poling, but the PL intensity varied similarly to the MEH-PPV, first decreased due to the electrets effect, and then increased PL due to stress-induced suppression of electron-phonon coupling. For the latter, greater PL enhancements were observed for the region-random polymer (r.r.=50%) in which the polymer chains are believed pulled more effectively by the polarization.

Interestingly, the fact that poling does not cause any shifting of the PL peaks indicates that the conjugation lengths were not altered by the poling. It implies that the molecular re-arrangement resulted from the poling was mainly due to that of the molecular segments corresponding to the conjugation length. It also indicates that the dominant dipoles induced during the poling are that of the π electrons along the delocalized backbones.

Further experiments on the dynamics of molecular re-arrangements are undergoing.

5. Molecular packing of conjugated molecules into ultrathin films

Molecular packing of conjugated polymer in ultrathin films is important for the optoelectronic behavior as well as the mechanical properties. Packing of the rigid-rod-type molecules of the conjugated polymers is expected to be deviated from that of flexible polymer chains such as PS. It is anticipated, however, that residual stress should also be

27

fostered during the process of spin coating of the rigid-rod macromolecules. Amid the molecular packing during solvent evaporation, molecular aggregates are expected to form with a certain level of bonding strength. The characteristics of chain entanglements of the rigid-rod polymers are also expected to be different from those of the flexible polymer chains such as PS. In this regards, supramolecular structures are expected to emerge in the thin films and the optoelectronic energy transfer pathways required more in-depth exploration.

By measuring the trench depth, the force exerting by the coated polymer film on the thick rubber substrate can be determined directly, which will then lead to the calculation of the residual stresses of the polymer film.

The initial results indicates that the approach is doable, such as the depth of the dewetting hole (Fig. 46) saturated at large hole diameter (Fig. 47), and the saturated hole depth increased with film thickness (Fig. 46), consistent with the increase of the residual force (residual stress times the thickness) with film thickness. The method of x-ray reflectivity was being used to probe the through-thickness microstructure of the thin films, to provide important information for the development of the residual stresses and the supramolecular structures. Further experiments are ongoing.

- 400K PS on thick PDMS, Annealing at 160°C
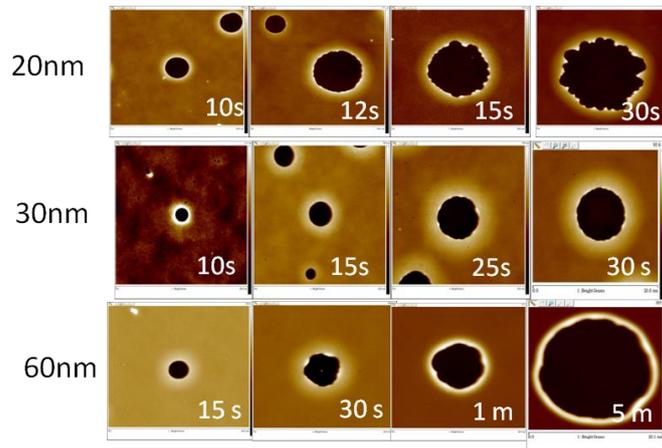
Figure 46. The AFM micrographs of the dewetting holes of the 400k PS of various thicknesses annealed at 160C on the thick PDMS substrate for measurements of the residual stresses.
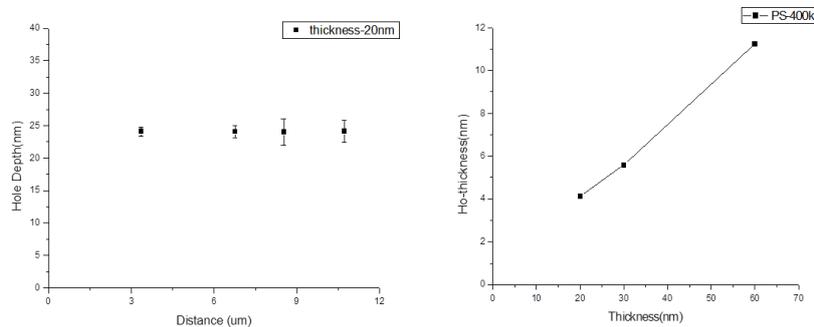
Figure 47. The hole depth versus hole diameter; the saturated hole depth versus the film thickness.

28
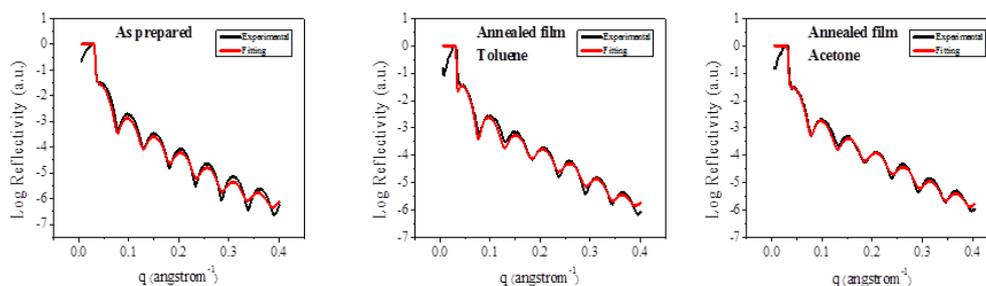
Figure 48. The x-ray reflectivity spectra of the thin polymer films for exploring the through-thickness microstructure.

Conclusions:

We may conclude that mechanical stresses exerting on conjugated polymer molecular strands can enhance the quantum efficiencies, via suppression of the electron-phonon coupling, not only for the dilute or single molecules, but also for the neat conjugated polymers. Small conjugated molecules also manifest a similar molecular stress effect but the molecular aggregation effect is substantially milder. Other means of suppressing the electron-phonon coupling via confining the molecular movements, such as intermolecular hydrogen bonding, can also be used to enhance the optoelectronic efficiencies. Exciton quenching can be reduced substantially by the application of large molecular stresses, indicating the fundamental role of electron-phonon interactions in the formation of excitons. By virtue of the strong electron-phonon coupling in conjugated polymers, light absorption can be used to manipulate molecular conformation and motions, which may be used to enhance optoelectronic efficiencies as well as for fine patterning.

List of Publications:

1. K. S. Shih, C. C. Chen, P.-T. Chen, Y.-W. Yang, J. D. White, Y.-M. Chang, A. C.-M. Yang, "Photoluminescence of MEH-PPV Brushes, Pancakes, and Free Molecules in Solutions and Dry States", *ACS Photonics*, in revision.
2. I. Botiz, P. Freyberg, C. Leordean, A.-M. Gabudean, S. Astilean, A. C.-M. Yang, N. Stingelin, "Enhancing the Photoluminescence Emission of Conjugated MEH-PPV by

Light Processing", *ACS Appl. Mater. Interfaces* **2014,** 6, 4974-4979.

3. P. Freyberg, C. Leordean, G. A. Maria, S. Astilean, A. C.-M. Yang, N. Stingelin, "Emission Properties of MEH-PPV in Thin Films Simultaneously Illuminated and Annealed at Different Temperatures", *Synthetic Metals* 2014, accepted.

4. Tsai-Ming Huang, Jin-You Lin, Le Anh Phuong, Orlando Marin, Chien-Neng Liao, Wha-Tzong Whang, Arnold C. -M. Yang, **2014**, "Ultra-Low Resistivity of Charge Transport in Ultrathin Polymer Films", in submission.

5. Y. L. Chang, Y. CHIEN, A. C.-Y. Chou, G. Reiter, A. C.-M. Yang, **2014**, "Molecular Packing of Long Polymer Chains in Ultrathin Films via Spin Casting", in submission.

Patent Application:

A. C.-M. Yang, Y. H. Liu, C. C. Cheng, C. C. Huang, "Conjugated polymer-based optoelectronic materials", Taiwan patent application, application number: 103127057; US patent application in preparation.

DD882 as a separate document was complete.